$K\beta$ satellite and forbidden transitions in elements with $12 \leqslant Z \leqslant 30$ induced by electron impact

Silvina P. Limandri,[1,2] Alejo C. Carreras,[1,3,*] Rita D. Bonetto,[1,4] and Jorge C. Trincavelli[1,2]

[1]*Consejo Nacional de Investigaciones Científicas y Técnicas, C1033AAJ Buenos Aires, Argentina*

[2]*Facultad de Matemática, Astronomía y Física, UNC, 5000 Córdoba, Argentina*

[3]*Instituto de Investigaciones en Tecnología Química, UNSL, CC290–5700 San Luis, Argentina*

[4]*Centro de Investigación y Desarrollo en Ciencias Aplicadas Dr. Jorge Ronco, FCE-FI-UNLP, CC59–1900 La Plata, Argentina*

(Received 2 October 2009; published 19 January 2010)

The emission of x rays in the $K\beta$ region of Mg, Al, Si, Sc, Ti, Cr, Fe, Ni, and Zn induced by electron bombardment was studied by means of wavelength dispersive spectroscopy. The lines studied were: the $K\beta^{\mathrm{III}}$ and $K\beta^{\mathrm{IV}}$ spectator hole transitions, the $1s \rightarrow 3s$ quadrupole decay, the $K\beta_2$ and $K\beta_5$ diagram transitions, the structures related to radiative Auger processes, and the $K\beta'$ and $K\beta''$ lines. Relative energies and probabilities were determined through a careful spectral processing based on a parameter refinement method. The results obtained were compared with other experimental and theoretical determinations when available.

DOI: 10.1103/PhysRevA.81.012504 PACS number(s): 32.30.Rj, 32.70.−n, 33.70.Jg, 34.80.Dp

I. INTRODUCTION

The emission of x rays in atomic relaxation processes provides valuable information about some features of atomic structure and certain molecular and solid-state effects. A detailed analysis of the fine structure of x-ray spectra involving decays from inner-shell hole atomic states reveals the existence of a number of different processes that can take place as relaxation mechanisms.

Single inner-shell vacancies lead to the emission of x rays and Auger electrons. The characteristic x rays emitted by atoms having initially one inner-shell vacancy that is filled by a full radiative process are called the diagram lines. Multiple ionization and different deexcitation mechanisms are the main processes responsible for the generation of the so-called satellite lines. The study of the satellite lines is of great interest since they provide information on intra-atomic electron correlation, excitation dynamics, relaxation, and other effects influencing the x-ray emission process.

Several works were carried out to investigate the K satellite transitions induced by photon [1–14], proton [15–18], heavy-ion [15,19–22], and electron [23–33] impact, although most of them are focused on a few particular elements or transitions. Theoretical calculations were performed by several authors [25,26,29,34–40]. Nevertheless, the experimental and theoretical results available show important discrepancies and leave certain areas unexplored, particularly for the $K\beta$ satellite lines.

The $K\beta$ region in pure elements mainly involves the most intense $K\beta_{1,3}$ diagram line, radiative Auger emissions, the $K \rightarrow M_1$ quadrupole decay, the $K\beta^{\mathrm{III}}$ and $K\beta^{\mathrm{IV}}$ double ionization processes, the $K\beta'$ and $K\beta''$ structures, and the $K\beta_2$ and $K\beta_5$ diagram transitions.

The radiative Auger effect (RAE) is a process competitive to the emission of the diagram line, in which the inner-shell hole is filled by a transition of an electron from an outer shell, resulting in the emission of a photon and another outer shell electron [14,41]. The emitted x-ray photon shares its energy with the ejected electron; therefore, it has an energy lower than the corresponding diagram line. The RAE broad structure has an energy distribution that is quite symmetric around a maximum called the RAE peak. The maximum energy of each of these bands is known as the RAE edge and it corresponds to an electron emitted with zero kinetic energy. A close relationship between the RAE energy distribution, and the absorption x-ray and Auger electron spectra was found earlier [42,43]. On the other hand, variations in the RAE intensity were studied for different Ti [44] and Fe compounds [45]. The RAE transitions, which follow a nomenclature similar to nonradiative Auger emissions, may lead to erroneous interpretation of spectra; for example, the energy corresponding to Fe RAE $KM_{2,3}M_1$ coincides with that of the cobalt $K\alpha$ diagram lines.

Low atomic number elements ($Z < 13$) have no $3p$ electrons in their ground states; then, in these elements the $1s \rightarrow 3p$ decay ($K\beta_{1,3}$ line) is not possible. In magnesium, there are two $3s$ electrons that can decay to fill a K vacancy giving rise to a characteristic KM_1 photon. This line, arising from a quadrupole transition, usually masked by the much more intense dipole decay $K\beta_{1,3}$, can be clearly observed in the Mg spectrum. The relative intensity corresponding to the quadrupole transition in the $K\beta$ spectrum should decrease with the atomic number from $Z = 12$ to $Z = 18$, according to the increase in the $3p$ level population (i.e., to the increase in the $K\beta_{1,3}$ line intensity).

The presence of a vacancy, or spectator hole, unfilled during a transition is responsible for the distortion of the atomic energy levels, and therefore, for the existence of certain satellite lines known as double ionization satellites. The energy and intensity of these lines depend on the spectator hole energy level and multiple ionization probability, respectively. Four mechanisms participate in the creation of spectator holes: shake-off, shake-up, two-step-one (TS1) and two-step-two (TS2) [33]. The first two are called one-step mechanisms and consist in the ejection of one atomic electron to the continuum (shake-off) or the excitation to a higher unoccupied bound state produced by a sudden change in the atomic potential occurring after an inner-shell ionization (shake-up). The last two processes are referred to as two-step mechanisms. In TS1 the electron ejected after the first collision interacts with

*Now at: Faculty of Basic Sciences, Hochschule Esslingen, University of Applied Sciences, Kanalstrasse 33, 73728 Esslingen, Germany.

another bound electron of the same atom creating a new vacancy. On the other hand, TS2 refers to a process in which both vacancies are generated sequentially by the same incident particle. For this reason, TS2 processes are not possible by photon excitation. The probability of one-step mechanisms is independent of the incident particle, whereas for two-step processes, it depends on the energy and kind of projectile.

The $K\beta^{\mathrm{III}}$ and $K\beta^{\mathrm{IV}}$ lines, investigated by a number of researchers [14–17,24,27,46,47] are originated from $1s \rightarrow 3p$ transitions in the presence of a $2p$ spectator vacancy. In electron and photon excited spectra of light elements, $K\beta^{\mathrm{IV}}$ is the most energetic and weakest line of the doublet. For increasing atomic numbers, both lines become closer and weaker. An additional nomenclature usual in the field of ion excitation, involves the name of the diagram line and the number and kind of spectator holes; in this case, $K\beta L^1$ refers to a $K\beta$ transition in the presence of one L spectator hole.

The structure usually known as $K\beta'$ is the main responsible for the asymmetric shape in the low-energy side of the diagram line $K\beta_{1,3}$ for $Z > 22$. It has been studied by several authors, although its origin is still under debate for transition metals. Some researchers state that, for this case, $K\beta'$ is generated by a $3p$ decay, accompanied by a plasmon excitation in the conduction band. The $K\beta_{1,3}$ energy is then shared between this plasmon and the emitted photon, giving rise to the lower energy line $K\beta'$ [48,49]. Tsutsumi *et al.* proposed an alternative explanation involving $3p3d$ shell exchange interaction [50]. All these interpretations suggest that the intensity of the $K\beta'$ line is not dependent on either the projectile kind or energy, but depends only on the subsequent relaxation process. On the other hand, several authors [51–54] state that in the $K\beta'$ region, the main mechanism responsible for this structure is a $3d$ spectator hole transition. Particularly, measurements carried out recently with photon excitation [53,54] in copper, where the exchange interactions are less important, indicate that the structure appearing in the $K\beta'$ region presents an intensity dependent on the excitation energy near the double ionization edge, supporting the last interpretation. The use of different particles as excitation sources could help to reveal the nature of this spectral region, since a different particle has a different probability to create a double vacancy state.

The satellite line $K\beta''$ distorting the high energy side of the diagram line may also be interpreted as due to the presence of a $3d$ spectator hole [53,54]. The origin of this transition for Ti and Cr has also been attributed to plasmon excitation produced by a $K\beta_5$ photon [55].

The $K\beta_5$ line arising from the $K \rightarrow M_{4,5}$ transition corresponds to a quadrupole term in the multipole expansion of the evolution operator (i.e, it is a forbidden transition according to the electric dipole selection rules). This, in fact, is entirely true for $Z > 30$, where M_4 and M_5 are inner shells. However, for lower atomic numbers, those levels are the outermost shells and the corresponding wave functions are affected by molecular bonds and solid-state effects. Therefore, for these lower Z elements, the $K\beta_5$ line is due to a transition involving molecular orbitals and then the dipolar term should be added to the quadrupole one. A careful measurement of $K\beta_5$:$K\beta_{1,3}$ intensity ratios is of great interest in view of the important discrepancies found in the available experimental data, particularly in the range of elements studied in this work [56]. The $K\beta_2$ line, which is close to the $K\beta_5$ transition for the elements in the fourth period, corresponds to a $K \rightarrow N_{2,3}$ decay.

In this work, the $K\beta$ transitions previously mentioned were studied for Mg, Al, Si, Sc, Ti, Cr, Fe, Ni, and Zn. An incident electron beam was used for vacancy generation and the x-ray detection was carried out with a wavelength dispersive spectrometer. A careful spectral processing was performed by means of a powerful homemade software presented previously [57]. The Z dependence of the energy shift and the intensity of several satellite lines relative to the corresponding diagram transitions were studied and compared with experimental and theoretical results, when available in the literature.

II. EXPERIMENT

X-ray K spectra were measured for elements with $12 \leqslant Z \leqslant 30$ with a LEO 1450 VP scanning electron microscope equipped with an INCA WAVE 700 wavelength dispersive spectrometer (WDS) from the Laboratorio de Microscopía Electrónica y Microanálisis (LABMEM) of the Universidad Nacional de San Luis, Argentina. The arrangement of the WDS is the Johansson type for the thallium acid phthalate (TAP), pentaerythritol (PET), and lithium fluoride (LiF) crystals used in this work. The spectra were collected from pure standards with a beam current of 110 nA and a takeoff angle of 29°. The other experimental conditions are summarized in Table I.

The spectral fitting was performed by means of the optimization routine implemented in the software POEMA [57]. This method consists of minimizing the differences between the experimental spectrum and an analytical function proposed to describe it, through the refinement of several parameters involved in the analytical spectrum. This function takes into account characteristic peaks, bremsstrahlung, and different detection artifacts. Characteristic emission was considered by evaluating the so-called ZAF corrections [atomic number (Z), absorption (A), and fluorescence (F)] with a line profile given by a Voigt function [58], whereas an empirical model was used to fit the bremsstrahlung [59]. For the detection efficiency of the spectrometer, a model developed previously was implemented [60]. A more detailed description of the spectral processing can be found in a previous publication [61].

All the $K\beta_{1,3}$ diagram lines were fitted with one Voigt function, except for silicon, for which two Voigt functions were necessary to achieve a good fit. The satellite lines were also fitted with one Voigt function except for RAE transitions and Fe $K\beta'$, for which Gaussian profiles were used due to their broad structures.

TABLE I. Experimental conditions for the analyzed spectra.

Element	Incidence energy (keV)	Crystal (plane)	Collimator slit size (mm)
Mg, Al	18	TAP (101)	2.5
Si	18	PET (002)	0.9
Sc, Ti	21	PET (002)	0.02
Cr, Fe, Ni, Zn	21	LiF (200)	0.02

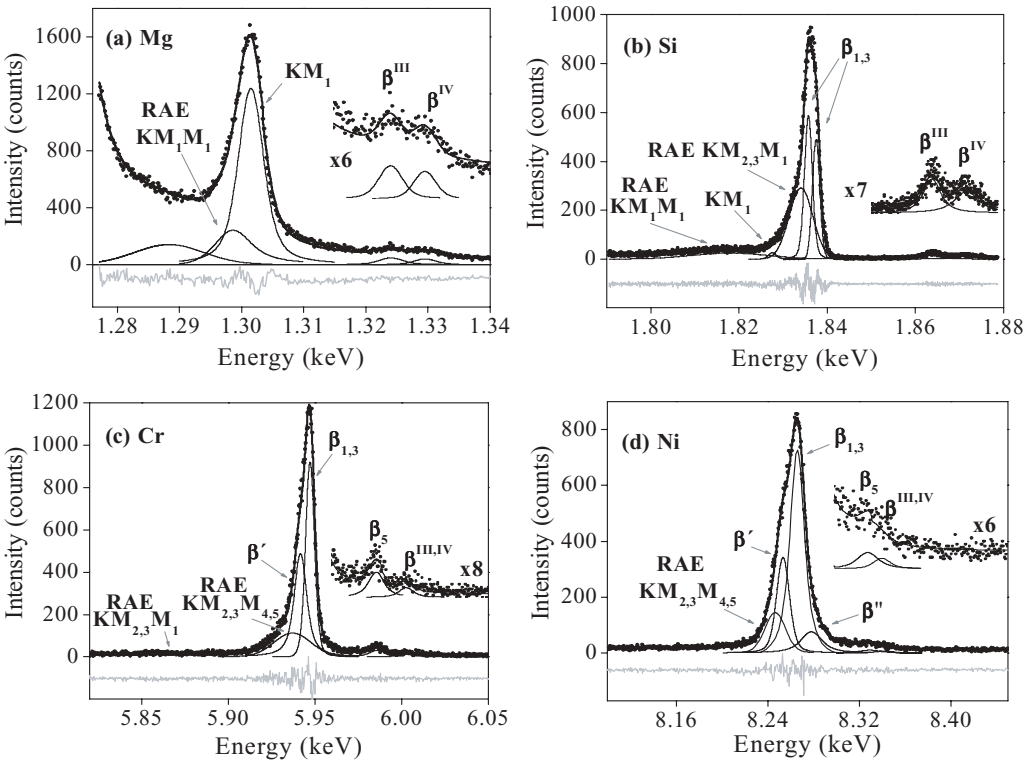

FIG. 1. (a) Magnesium, (b) silicon, (c) chromium, and (d) nickel $K\beta$ spectra. (Dots) Experimental spectra; (thick solid line) fitting; and (gray thick line) the difference between experimental and analytical spectra. The different satellite and diagram lines are indicated in each figure with thin solid lines. The name "$K\alpha$ sat." denotes a structure whose cause could be a satellite $K\alpha$ transition.

III. RESULTS AND DISCUSSION

In Fig. 1, the structure of the $K\beta$ spectrum can be seen for magnesium, silicon, chromium, and nickel. These spectra were chosen as examples among the elements studied, since they involve the different kinds of lines and bands present in the whole set. A good fit of the experimental spectra can be observed.

The energies and transition probabilities obtained are presented in Tables II–IV. The parameter refinement was performed keeping fixed the energy of the main diagram $K\beta_{1,3}$ line for Sc, Ti, Cr, Fe, Ni, and Zn, and the $K\alpha_1$ energy for Mg, Al, and Si, for which the values published by Bearden [62] were used. Regarding the transition probabilities obtained, they are relative to the whole $K\beta$ spectrum in all the cases.

A. Radiative Auger transitions

The results obtained are shown in Fig. 2. Three different RAE transitions (KM_1M_1, $KM_{2,3}M_1$, and $KM_{2,3}M_{4,5}$) were assigned for the elements studied. This assignment was performed with the help of data previously published (when available) and by comparing the peak shift respect to the $K\beta_{1,3}$ line, with the binding energy of the ejected Auger electron.

When the relaxation energy following a $K \rightarrow M_i$ transition is shared between a photon of energy $h\nu$ and an Auger electron ejected from the M_j shell with kinetic energy E_{el}, the energy

TABLE II. Energies (E) and transition probabilities relative to the $K\beta$ group (RTP) for Mg, Al, and Si. The name "$K\alpha$ satellite" is provisory. Numbers in parentheses are the estimated uncertainties in the last digit.

	Mg		Al		Si	
Transition	E (keV)	RTP	E (keV)	RTP	E (keV)	RTP
$K\alpha$ satellite	1.287(4)	0.11(2)				
$K\beta_{1,3}$			1.5577(1)	0.70(6)	1.836(2)[a]	0.44(8)[a]
RAE KM_1M_1	1.2985(4)	0.20(5)	1.555(1)	0.22(4)	1.8177(5)	0.095(8)
RAE $KM_{2,3}M_1$					1.834(1)	0.33(2)
KM_1	1.30126(3)	0.56(1)			1.8275(3)	0.012(3)
$K\beta^{III}$	1.3241(5)	0.080(7)	1.5852(4)	0.09(1)	1.8638(9)	0.069(9)
$K\beta^{IV}$	1.3295(5)	0.059(6)			1.8717(1)	0.062(9)

[a]Transition fitted by two Voigt functions. A mean energy was estimated by averaging both maxima weighted by their corresponding areas. The RTP value was obtained by adding both RTPs.

TABLE III. Energies (E) and transition probabilities relative to the $K\beta$ group (RTP) for Sc, Ti, and Cr. Numbers in parentheses are the estimated uncertainties in the last digit.

	Sc		Ti		Cr	
Transition	E (keV)	RTP	E (keV)	RTP	E (keV)	RTP
$K\beta_{1,3}$	4.4605[a]	0.950(5)	4.93181[a]	0.964(6)	5.94671[a]	0.49(1)
RAE $KM_{2,3}M_1$	4.398(1)	0.0139(8)	4.857(1)	0.0112(2)	5.855(5)	
RAE $KM_{2,3}M_{4,5}$					5.937(1)	0.13(1)
$K\beta^{\mathrm{III,IV}}$	4.5135(5)	0.019(1)	4.989(2)	0.0078(9)	6.0026(8)	0.015(2)
$K\beta'$					5.9413(6)	0.33(2)
$K\beta_5$	4.4878(3)	0.0165(8)	4.9634(6)	0.017(1)	5.9854(4)	0.032(2)

[a]Characteristic energies according to Ref. [62].

balance can be written as

$$h\nu + E_{el} = E(K) - E(M_i) - E(M_j), \tag{1}$$

where the terms in the second member refer to K, M_i, and M_j binding energies, respectively.

The RAE edge E_e is the maximum photon energy emitted in a RAE process, corresponding to an Auger electron ejected with zero kinetic energy, as mentioned in Sec. I, therefore

$$E_e = E(K) - E(M_i) - E(M_j). \tag{2}$$

This edge is, thus, the difference between the energy of the diagram line and the Auger electron binding energy. The energy of the RAE band maximum E_m is always a few eV below this edge. For the case of RAE associated with $K\beta_{1,3}$ transitions, Eq. (2) can be written as:

$$E_m \cong E_e = E(K\beta_{1,3}) - E(M_j), \tag{3}$$

where $E(K\beta_{1,3})$ is the energy of the $K\beta_{1,3}$ line.

In the case of Mg, instead, the unique RAE KMM transition possible involves only the M_1 shell, since both Mg outermost electrons belong to the $3s$ level. The corresponding absorption energy $E(M_1)$ is difficult to obtain; for instance, if the energy of the transition $L_{2,3} \rightarrow M_1$ and the $L_{2,3}$ absorption edge given by Bearden [62] are used, a value of 0.43 eV is achieved, whereas if the absorption edge is taken from the work of Bearden and Burr [63], the binding energy $E(M_1)$ derived is 2.1 eV. On the other hand, Perkins *et al.* [64] published a value of 6.89 eV for this energy level. Taking into account that the E_m value obtained in this work for Mg is 2.8 eV less than the KM_1 energy (see Table II), and bearing in mind the great uncertainty in the estimation of $E(M_1)$, the band closest to the KM_1 main line shown in Fig. 1(a) can be reasonably attributed to a RAE KM_1M_1 transition. Another structure can be observed for Mg with a maximum at 14.3 eV less than the main peak. This band cannot be either a RAE KMM or KLM, since Mg $E(L_{2,3})$ is 51.4 eV [63]. A possible cause for this transition could be a $K\alpha$ satellite, and it should be investigated with more detail. Also for aluminum, a KM_1M_1 band was the only RAE transition observed (see Table II), even when there is a $3p$ electron in this element; nevertheless, it cannot be stated that there is no other RAE band for aluminum, since the statistics for the corresponding measured spectrum was lower than for the other ones. Two RAE transitions were studied for silicon: KM_1M_1 and $KM_{2,3}M_1$, as can be seen in Fig. 1(b). For Sc and Ti, only the RAE $KM_{2,3}M_1$ band was observed, while for Cr the RAE $KM_{2,3}M_{4,5}$ transition was also found very close to the main line $K\beta_{1,3}$ [see Fig. 1(c)]. Finally, for Fe, Ni, and Zn, the $KM_{2,3}M_{4,5}$ structure was the only RAE observed [Fig. 1(d)].

The assignation of the RAE peaks observed to specific RAE transitions is not straightforward. It must be noted that the RAE KM_iM_j maximum energy E_m relative to the main $K\beta$ line cannot exceed the value $-E(M_j)$ [see Eq. (2)]. For the particular case of RAE KM_1M_1 transitions in Al and Si, the energy shifts with respect to the $K\beta_{1,3}$ line cannot be greater than $E(M_{2,3}) - 2E(M_1)$. These upper limits are

TABLE IV. Energies (E) and transition probabilities relative to the $K\beta$ group (RTP) for Fe, Ni, and Zn. Numbers in parentheses are the estimated uncertainties in the last digit.

	Fe		Ni		Zn	
Transition	E (keV)	RTP	E (keV)	RTP	E (keV)	RTP
$K\beta_{1,3}$	7.05798[a]	0.59(2)	8.26466[a]	0.58(1)	9.5720[a]	0.47(4)
RAE $KM_{2,3}M_{4,5}$	7.043(1)	0.174(8)	8.243(1)	0.076(4)	9.540(1)	0.061(4)
$K\beta^{\mathrm{III,IV}}$	7.119(2)	0.010(2)	8.3401(6)	0.007(5)		
$K\beta'$	7.048(1)	0.20(3)	8.2522(5)	0.23(1)	9.555(3)	0.22(2)
$K\beta''$			8.277(2)	0.099(5)	9.5953(6)	0.23(2)
$K\beta_2$[b]					9.6580[a]	0.003(2)
$K\beta_5$	7.106(1)	0.020(2)	8.328(1)	0.013(4)	9.6501[a]	0.016(4)

[a]Characteristic energies according to Ref. [62].
[b]Transition assigned to the $K\beta_2$ decay according to Ref. [62].

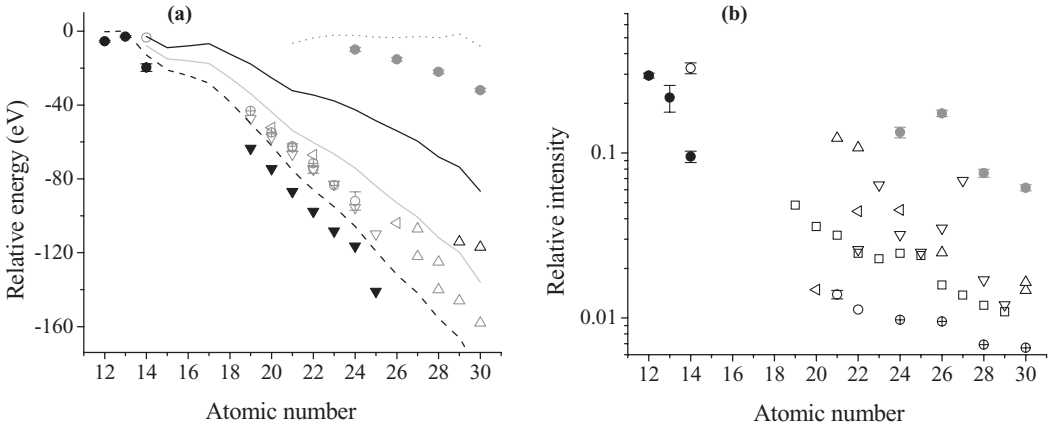

FIG. 2. Parameters related to the RAE transitions as a function of the atomic number. The point shape indicates the different excitation modes: electrons (circles); protons and heavy ions (squares), and photons (triangles), while their color denotes the specific RAE transition: KM_1M_1 (black solid symbols), $KM_{2,3}M_1$ (gray open symbols), $KM_{2,3}M_{2,3}$ (black open symbols), and $KM_{2,3}M_{4,5}$ (gray solid symbols). (a) Energy shift with respect to $K\beta_{1,3}$. Circles: present results; crossed circles: Ref. [66]; up triangles: Ref. [68]; left triangles: Ref. [9]; and down triangles: Ref. [14]. Lines correspond to the M-edge energies (see text): $E(M_{2,3}) - 2E(M_1)$ (dashed line); $-E(M_1)$ (gray solid line); $-E(M_{2,3})$ (black solid line); and $-E(M_{4,5})$ (dotted line). (b) Intensity relative to the $K\beta$ group. Circles: present results; crossed circles: Refs. [67] for $Z = 24$ and 26 and [68] for $Z = 28$ and 30; up triangles: Ref. [65]; left triangles: Ref. [9]; down triangles: Ref. [70]; and squares: Ref. [69].

shown in Fig. 2(a), where the M_j absorption edges were introduced, according to data published by Bearden and Burr [63], completing the lacking data with values obtained from KM_1M_1 Auger [65] and $K\beta_{1,3}$ energies [62]. The difference between the maximum energy relative to the main $K\beta$ peak and its corresponding upper limit is approximately the RAE peak half-width; bearing this in mind and considering the experimental widths achieved, the assignation of each RAE transition can be done.

Due to the experimental resolution, the RAE transitions interpreted as $KM_{2,3}M_1$ in the present work include the contributions made by KM_1M_1 and $KM_{2,3}M_{2,3}$ for Sc, Ti, and Cr. These three RAE structures have been studied by several authors [9,14,65–70], although only in the last four works relative intensities are reported, where the contributions given by KM_1M_1, $KM_1M_{2,3}$, and $KM_{2,3}M_{2,3}$ are also considered together. Even when in Refs. [65,67] information about energies is given, they refer to RAE edges instead of E_m values. As can be seen from Fig. 2(a), the RAE relative energy data presented here are in agreement with the values published by the other authors.

Regarding KM_1M_1 peak energies, up to our knowledge neither experimental nor theoretical data are available for Mg, Al, and Si. The E_m values presented here for these elements behave similarly to their expected upper limits, keeping themselves slightly below them; in addition, these data seem to follow the trend observed by Raju *et al.* [14] for heavier elements.

Regarding the RAE $KM_{2,3}M_{4,5}$ structure, it must be born in mind that the determination of its energy and intensity could depend on the fitting criterion, since this band interferes with the $K\beta'$ structure. Therefore, the identification of these transitions in the spectra is not free of certain ambiguity, considering the experimental resolution and due to the lack of data in the literature, which would allow one to fix some parameters characteristic of these lines.

The RAE intensities relative to the $K\beta$ group are shown in Fig. 2(b) along with experimental results published by the authors previously mentioned. The decreasing behavior with Z shown for each RAE studied, agrees with the decrease of the Auger emission probability with the atomic number. Data of RAE relative intensities are even scarcer than the corresponding characteristic energies. Moreover, some authors [9,70] cannot discriminate the contributions of the different M levels to the RAE emission due to their limited experimental resolution. For these reasons, it is difficult to perform a direct comparison with the data presented in this work. The values reported by Verma [9] as RAE KMM were assigned to RAE $KM_{2,3}M_1$ due to their position in the spectrum. It can be seen from Fig. 2(b) that the data published by Bé *et al.* [70] and Verma [9] present a different behavior than the values reported by Servomaa and Keski-Rahkonen [67], Keski-Rahkonen and Ahopelto [68], Johansson *et al.* [69], and the ones presented here.

B. $1s \rightarrow 3s$ quadrupole transition

The $1s \rightarrow 3s$ decay, forbidden by the dipole selection rules is the only diagram transition possible for Mg in the $K\beta$ region. For increasing atomic numbers, this line begins to be hidden by the much more intense $K\beta_{1,3}$ peak ($1s \rightarrow 3p$). Nevertheless, for silicon, the forbidden transition can still be observed at 1.8275 keV [see Fig. 1(b)]. The $1s \rightarrow 3p$ characteristic energy calculated from the K (1.8400 keV [62]) and M_1 (0.0135 keV [64]) absorption edges is 1.8265 keV, which is in agreement with our determination. This forbidden decay was not observed for aluminum due to the lower statistics of the corresponding spectrum.

C. $2p$ spectator hole $K\beta^{III}$ and $K\beta^{IV}$ transitions

For the $K\beta^{III}$ and $K\beta^{IV}$ lines, the experimental resolution and the statistics of the measured spectra allow one to separate

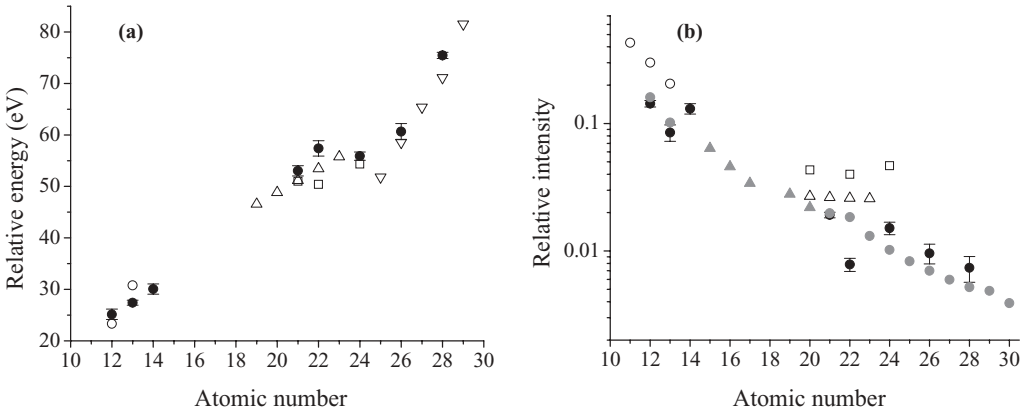

FIG. 3. Parameters related to the $K\beta^{\mathrm{III,IV}}$ group as a function of the atomic number. The point shape indicates the different excitation modes: electrons (circles); protons and heavy ions (squares), and photons (triangles). (a) Energy shift with respect to $K\beta_{1,3}$. Solid circles: present results; open circles: Ref. [24] for $Z = 13$ and Ref. [27] for $Z = 12$; squares: Ref. [17] for $Z = 22$ and 24 and Ref. [15] for $Z = 21$; up triangles: Ref. [14]; and down triangles: Ref. [47]. (b) Intensity relative to the $K\beta$ group. Black solid circles: present results; black open circles: Ref. [27]; black open up triangles: Ref. [14]; and black open squares: Ref. [17]. Gray symbols correspond to the experimental data of the $K\alpha_{3,4}$ intensity relative to the $K\alpha$ group. Solid circles: Ref. [23] for Z = 21–30 and Ref. [71] for $Z = 12$ and 13; and solid triangles: Ref. [3].

both peaks only for Mg and Si [see Figs. 1(a) and 1(b)], while one $K\beta^{\mathrm{III,IV}}$ peak was fitted for each of the other elements studied [see Figs. 1(c) and 1(d)]. The energy shift with respect to the $K\beta_{1,3}$ line and the intensity relative to the $K\beta$ group are plotted as a function of Z in Figs. 3(a) and 3(b), respectively. For Mg and Si, the data plotted are the average energy weighted by the intensities [(Fig. 3(a)] and the sum of $K\beta^{\mathrm{III}}$ and $K\beta^{\mathrm{IV}}$ relative intensities [Fig. 3(b)]. As can be seen, the energy values plotted are in agreement with experimental determinations carried out by means of electron, photon, and ion excitation. On the other hand, the intensities shown are quite different from the data obtained by means of other excitation sources, as expected. The excitation with protons and ions produces more intense double ionization satellites, since the probability of multiple vacancy creation by TS2 processes is higher in this case as compared to electron impact. For electron excitation, the only intensity values found in the literature were for Na and Mg with 6-keV electrons and Al with 3.25-keV electrons [27]. Regarding photon sources, for Z between 19 and 25, the values obtained by Raju *et al.* [14] with a Rh x-ray tube are also displayed in Fig. 3(b). Finally, data measured by Uri *et al.* [17] for Ca, Ti, and Cr with 2-MeV proton excitation are included.

In view of the availability of data for the $K\alpha_{3,4}\,2p$ spectator hole satellites as compared to the scarcer $K\beta^{\mathrm{III,IV}}$ experimental values, it is useful to find a relation between them. Taking into account that $K\beta^{\mathrm{III,IV}}$ intensity is proportional to the probability of double vacancy creation, and assuming that the probability of $K\alpha$ and $K\beta$ emission is (in a first approximation) unaffected by the presence of a spectator hole, the $K\beta^{\mathrm{III,IV}}$:$K\beta$ and $K\alpha_{3,4}$:$K\alpha$ relative intensities should be the same. In Fig. 3(b), $K\alpha_{3,4}$:$K\alpha$ experimental values obtained by other authors by photon (Rh x-ray tube) [3] and electron impact [23,71] are included. As can be seen, they present a behavior similar to the $K\beta^{\mathrm{III,IV}}$:$K\beta$ data obtained in this work. It must be mentioned that the values presented here for Al and Ti, somewhat below the general trend, were obtained from spectra with lower statistics than the other ones.

D. $K\beta'$ and $K\beta''$ transitions

In the present work, the structure closest to the $K\beta_{1,3}$ line contributing to its low-energy asymmetric tail is denoted by $K\beta'$ regardless of its origin. Within the great dispersion of experimental and theoretical data, the $K\beta'$ energy shift relative to the $K\beta_{1,3}$ peak [Fig. 4(a)] would seem to increase with Z up to $Z = 25$, whereas there is no general trend for higher atomic numbers. In this Z range, according to the data presented in this work, the shift keeps increasing with Z; experimental results published by Bearden and Shaw [47] and theoretical calculations made by Salem *et al.* [25] show the opposite behavior, while the experimental data obtained by these authors and the theoretical results given by Srivastava *et al.* [48] do not follow any clear trend. Regarding the $K\beta'$:$K\beta$ relative intensities, the dispersion of experimental and theoretical data is also very important [Fig. 4(b)]; the only data sets showing certain agreement are the ones presented here with the calculations performed by Srivastava *et al.* [48]. Even when the proximity between the $K\beta'$ line and the RAE $KM_{2,3}M_{4,5}$ band makes difficult the deconvolution of this spectral region, as mentioned in Sec. IIIA, it seems to be clear that the theoretical calculations carried out by Salem *et al.* [25], based on exchange interaction effects, are well above the results presented here, as well as the other values available in the literature. Nevertheless, more recent calculations [72,73] also performed in the frame of exchange interactions for compounds are in better agreement with the experimental results. It would be of interest to carry out these *ab initio* calculations for pure metals to obtain more reliable theoretical relative intensities.

The $K\beta''$ line corresponds to a transition less studied than the previous one. Several authors [51,53,54,74] attribute its origin to the presence of a $3d$ spectator hole for the particular case of copper. On the other hand, Gokhale *et al.* [55] proposed plasmon excitation as the origin of this transition for Ti and Cr. In this work, that transition was observed only for Ni and Zn. As can be calculated from the data published by Deutsch

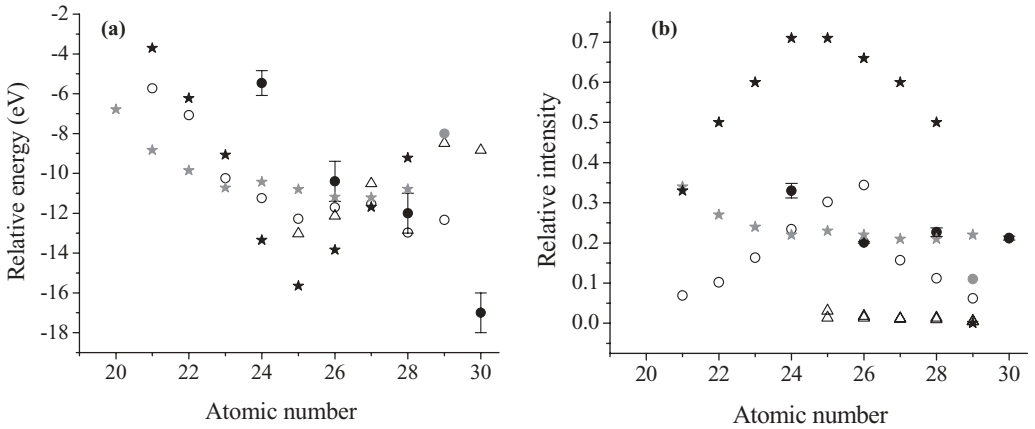

FIG. 4. Parameters related to the $K\beta'$ line as a function of the atomic number. The point shape indicates the different excitation modes: electrons (circles) and photons (triangles). Solid circles: present results; open circles: Ref. [25]; solid gray circle: Ref. [54]; and triangles: Ref. [47]. Theoretical results given in Refs. [25] (black stars) and [48] (gray stars) are also plotted. (a) Energy shift with respect to $K\beta_{1,3}$. (b) Intensity relative to the $K\beta$ group.

et al. [51], the $K\beta'':K\beta$ relative intensity is equal to 0.16 for Cu, while the corresponding values for Ni and Zn presented in Table IV are 0.099 and 0.23, respectively. These results show a behavior increasing with Z, although more elements should be studied to find a more reliable trend. On the other hand, values measured by Bearden and Shaw [47] exhibit a similar behavior although they are one order of magnitude lower, which leads to doubt about their fitting procedure. The energy shifts with respect to the $K\beta_{1,3}$ line obtained in this work for Ni and Zn (see Table IV) are sensibly greater than the value 5.4 eV obtained from Ref. [54] for Cu, whereas the value measured by Bearden and Shaw [47] for Zn coincides with the one obtained here within the experimental uncertainties.

E. $K\beta_2$ and $K\beta_5$ transitions

The energy of $K\beta_5$ with respect to the main $K\beta_{1,3}$ line and the intensity relative to the $K\beta$ group are shown in Figs. 5(a) and 5(b), respectively, along with data published by other authors. As can be seen, there is a very good agreement for the energies, whereas some discrepancies arise for the intensities. In relation to the latter, data corresponding to Asada *et al.* [75], Blokhin and Svejcer [76], and Török *et al.* [56] were obtained from the Fig. 4 published in Ref. [56]. According to the first two data sets, the $K\beta_5$ intensity decreases monotonically with Z, while Refs. [17] and [56] exhibit an opposite behavior for Z between 20 and 24. In addition, this intensity presents a maximum for Cr according to Meyer [77]; the values presented here corroborate this behavior. A maximum for the $K\beta_5$ intensity is expectable in the range of elements studied, since for Z above 20 the $3d$ shell begins to fill; nevertheless, if Z exceeds the value 24, the $3d$ electrons begin to pair up and the molecular bonding and solid-state effects involving this shell becomes weaker. Thus, the $K\beta_5$ line is weak for both lower and higher atomic numbers due to the lack of electrons and to the dipole selection rules, respectively; instead, in the intermediate region of the range studied, the $K\beta_5$ transition is more probable.

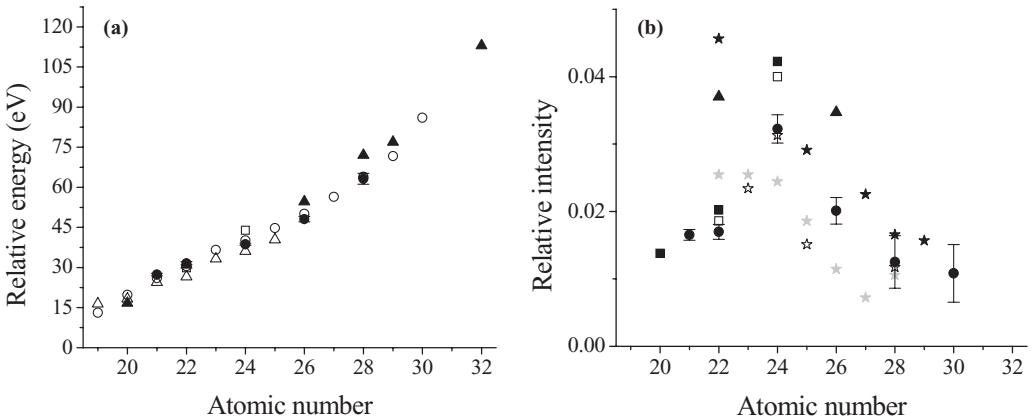

FIG. 5. Parameters related to the $K\beta_5$ line as a function of the atomic number. The point shape indicates the different excitation modes: electrons (circles), ions (squares), and photons (triangles). Solid circles: present results. (a) Energy shift with respect to $K\beta_{1,3}$. Open circles: Ref. [62]; solid triangles: Ref. [53] ($Z = 29$) and [9] ($Z = 26$, 28, and 32); open triangles: Ref. [14]; squares: Ref. [17]. (b) Intensity relative to the $K\beta$ group. Open squares: Ref. [17]; solid triangles: Ref. [9]; solid squares: Ref. [56]. Data compiled by Török *et al.* [56] corresponding to experimental values obtained: Refs. [76] (gray stars), [75] (black stars), and [77] (open stars) are also plotted.

According to the well-established x-ray wavelengths published by Bearden [62], implemented in several data bases [78,79], the line at 9.658 keV in the Zn spectrum corresponds to a $K\beta_2$ transition. Nevertheless, there is no clear reason to perform such identification, since this transition corresponds to a $K \rightarrow N_{2,3}$ decay, but Zn has no $N_{2,3}$ electrons in the ground state. In order to investigate this line, a peak was fitted at 9.658 keV (as suggested by Bearden [62]). The energy shift proposed and the relative intensity obtained follow the trend shown by the $K\beta^{\mathrm{III,IV}}$ line (see Tables II– IV). Therefore, it can be inferred that this line is due to a $3p$ spectator hole decay instead of the $K\beta_2$ diagram transition.

IV. CONCLUSION

Several $K\beta$ lines of nine elements with $12 \leqslant Z \leqslant 30$ were studied by means of electron incidence and wavelength dispersive x-ray spectroscopy. Relative energies and probabilities of KM_1M_1, $KM_{2,3}M_1$, and $KM_{2,3}M_{4,5}$ RAE transitions, $K\beta^{\mathrm{III}}$, $K\beta^{\mathrm{IV}}$, $K\beta'$, and $K\beta''$ satellites, $1s \rightarrow 3s$ and $K\beta_5$ dipole forbidden decays, and the weak diagram line $K\beta_2$ were determined by a careful spectral processing. It must be emphasized that for 17 (of the 37) energies and for 22 (of the 44) intensities determined, no data obtained with electron excitation were published in previous works, up to our knowledge. Moreover, for 10 transition energies and 15 relative intensities no data produced by any excitation source were found in the literature.

The energy shifts presented here are in good agreement with other theoretical and experimental values, where previous data are available, and they follow the general behavior as a function of the atomic number, when a trend can be observed in spite of the lack of values previously published. Regarding relative intensities, the present measurements are a contribution of interest, since the experimental data available are rather spread out.

Sometimes it is difficult to decide which particular RAE transition is associated to each RAE structure in the experimental spectrum. It is useful to compare the maximum RAE energy with the main line, since their difference cannot exceed the corresponding Auger electron binding energy.

The assumption that $K\beta$:$K\alpha$ relative transition probability is unaffected by the presence of a spectator hole was experimentally corroborated by comparing the $K\beta^{\mathrm{III,IV}}$:$K\beta$ and $K\alpha_{3,4}$:$K\alpha$ relative intensities, which exhibit the same behavior. For these $K\beta$ satellite lines, the relative intensity decreases with Z and is greater for heavy-ion or proton incidence. This behavior is related to the inner-shell multiple vacancy production, which becomes less probable for heavier atoms and increases with the mass and charge of the incident particle. On the other hand, the $K\beta^{\mathrm{III,IV}}$ energy shift with respect to the $K\beta_{1,3}$ line increases with Z. This behavior can be explained considering that the presence of a $2p$ spectator hole distorts more the atomic energy levels for greater nuclear charge. Nevertheless, this effect does not increase smoothly with Z, but seems to depend on the energy level filling order; particularly, a diminution in this distortion, reflected in the $K\beta^{\mathrm{III,IV}}$ energy shift, is observed for Cr ($Z = 24$), which suddenly changes its electronic configuration with respect to V ($Z = 23$).

The maximum for Cr in the relative $K\beta_5$ intensity presented in the compilation performed by Török *et al.* [56] was corroborated by the measurements carried out in the present work. This maximum is explained by the combination of two effects for increasing atomic numbers: on the one hand, the higher $3d$ population and, on the other hand, the decreasing participation of $3d$ orbitals in molecular bonds and solid-state effects.

According to the general trend followed by the $K\beta^{\mathrm{III,IV}}$ for all the elements studied, the line usually attributed to a $K\beta_2$ diagram decay for Zn [62], was assigned to a $3p$ spectator hole transition. Contrary to the commonly adopted assignation, this line identification permits one to keep the hypothesis of atom in the ground state.

Regarding $K\beta'$ and $K\beta''$ structures, whose origin has been explained by the contribution of different effect, measurements with different excitation sources and different incidence energies far from the K edge to avoid possible fine structure effects, would be of interest. This kind of experiment would be useful to reveal to what extent the intensity of these lines depend on the projectile, which would throw some light on their origin.

ACKNOWLEDGMENTS

The authors gratefully acknowledge the Laboratorio de Microscopía Electrónica y Microanálisis of the Universidad Nacional de San Luis, Argentina, where measurements were carried out. The authors thank Dr. G. Stutz for his helpful comments. Financial support from the Consejo Nacional de Investigaciones Científicas y Técnicas and the Agencia Nacional de Promoción Científica y Tecnológica of the Argentine Republic is also acknowledged.

[1] G. Graeffe, H. Juslén, and M. Karras, J. Phys. B: Atom. Molec. Phys. **10**, 3219 (1977).

[2] P. Chevallier, M. Tavernier, and J. Briand, J. Phys. B , **11**, L171 (1978).

[3] G. R. Babu, V. Gopalakrishna, M. N. L. Raju, K. Parthasaradhi, V. R. K. Murty, M. V. R. Murti, and K. S. Rao, Phys. Rev. A **36**, 386 (1987).

[4] H. Sorum, J. Phys. F **17**, 417 (1987).

[5] M. Fritsch, C. C. Kao, K. Hämäläinen, O. Gang, E. Förster, and M. Deutsch, Phys. Rev. A **57**, 1686 (1998).

[6] V. R. K. Murty, K. Parthasaradhi, and M. V. R. Murti, X-Ray Spectrom. **27**, 23 (1998).

[7] D. F. Anagnostopoulos, G. Borchert, D. Gotta, K. Rashid, D. H. Jakubassa-Amundsen, and P. A. Amundsen, Phys. Rev. A **58**, 2797 (1998).

[8] O. Mauron, J. C. Dousse, J. Hoszowska, J. P. Marques, F. Parente, and M. Polasik, Phys. Rev. A **62**, 062508 (2000).
[9] H. Verma, J. Phys. B **33**, 3407 (2000).
[10] K. Kawatsura, T. Morikawa, K. Takahiro, M. Oura, H. Yamaoka, K. Maeda, S. Hayakawa, S. Ito, M. Terasawa, and T. Mukoyama, J. Phys. B **36**, 4065 (2003).
[11] N. Shigeoka, H. Oohashi, T. Tochio, Y. Ito, T. Mukoyama, A. M. Vlaicu, and S. Fukushima, Phys. Rev. A **69**, 052505 (2004).
[12] R. Diamant, S. Huotari, K. Hämäläinen, R. Sharon, C. C. Kao, and M. Deutsch, Radiat. Phys. Chem. **75**, 1434 (2006).
[13] K. Yokoi, H. Oohashi, Y. Ito, T. Tochio, and T. Shoji, Radiat. Phys. Chem. **75**, 1461 (2006).
[14] S. S. Raju, B. Seetharami Reddy, M. V. R. Murti, and L. Mombasawala, X-Ray Spectrom. **36**, 35 (2007).
[15] B. Hodge, R. Kauffman, C. F. Moore, and P. Richard, J. Phys. B **6**, 2468 (1973).
[16] M. K. Kavi, M. Budnar, A. Mühleisen, and I. Török, Nucl. Instrum. Methods B **136-138**, 173 (1998).
[17] M. Uri, M. Kavi, and M. Budnar, Nucl. Instrum. Methods B **211**, 7 (2003).
[18] M. Kavcic, Phys. Rev. A **68**, 022713 (2003).
[19] K. Jamison, C. Woods, R. Kauffman, and P. Richard, Phys. Rev. A **11**, 505 (1975).
[20] K. Jamison, J. Hall, J. Oltjen, C. Woods, R. Kauffman, T. Gray, and P. Richard, Phys. Rev. A **14**, 937 (1976).
[21] I. Török, T. Papp, and S. Raman, Nucl. Instrum. Methods B **150**, 8 (1999).
[22] I. Török and T. Bondár, Nucl. Instrum. Methods B **154**, 272 (1999).
[23] L. Parrat, Phys. Rev. **50**, 1 (1936).
[24] D. Fischer and W. Baun, J. Appl. Phys. **36**, 534 (1965).
[25] S. Salem, G. Hockney, and P. Lee, Phys. Rev. A **13**, 330 (1976).
[26] N. Maskil and M. Deutsch, Phys. Rev. A **38**, 3467 (1988).
[27] O. Keski-Rahkonen, E. Mikkola, K. Reinikainen, and M. Lehkonen, J. Phys. C **18**, 2961 (1985).
[28] U. Misra and L. Watson, Phys. Scr. **36**, 673 (1987).
[29] S. I. Salem and B. L. Scott, Phys. Rev. A **35**, 1607 (1987).
[30] S. Soni, Phys. Lett. **A237**, 48 (1997).
[31] G. Hölzer, M. Fritsch, M. Deutsch, J. Härtwig, and E. Förster, Phys. Rev. A **56**, 4554 (1997).
[32] D. Küchler, U. Lehnert, and G. Zschornack, X-Ray Spectrom. **27**, 177 (1998).
[33] O. Mauron and J. C. Dousse, Phys. Rev. A **66**, 042713 (2002).
[34] F. A. Gianturco, J. Phys. B (Proc. Phys. Soc) **1**, 614 (1968).
[35] B. Hodge, Phys. Rev. A **16**, 1543 (1977).
[36] M. Deutsch, Phys. Rev. A **39**, 1077 (1989).
[37] M. Deutsch, Phys. Rev. A **39**, 3956 (1989).
[38] J. Kawai, J. Electron Spectrosc. Relat. Phenom. **101–103**, 847 (1999).
[39] T. Mukherjee and P. Mukherjee, Phys. Scr. **59**, 219 (1999).
[40] M. Kavi and K. Tőkési, Rad. Phys. Chem. **76**, 542 (2007).
[41] A. N. Nigam and S. N. Soni, J. Phys. C **14**, 3289 (1981).
[42] J. Kawai, Anal. Sci. **21**, 733 (2005).
[43] I. Abrahams, L. Kövérb, J. Tóth, D. S. Urch, B. Vrebos, and M. West, J. Electron Spectrosc. Relat. Phenom. **114–116**, 925 (2001).
[44] J. Kawai, T. Nakagima, T. Inoue, H. Adachi, M. Yamaguchi, K. Maeda, and S. Yabuki, Analyst **119**, 601 (1994).
[45] M. Kasrai and D. S. Urch, Chem. Phys. Lett. **53**, 539 (1978).
[46] S. N. Soni, J. Phys. Chem. Solids **57**, 1831 (1996).
[47] J. A. Bearden and C. H. Shaw, Phys. Rev. **48**, 18 (1935).
[48] K. S. Srivastava, S. Singh, A. K. Srivastava, R. S. Nayal, A. Chaubey, and P. Gupta, Phys. Rev. A **25**, 2838 (1982).
[49] A. S. Koster and H. Mendel, J. Phys. Chem. Solids **31**, 2511 (1970).
[50] K. Tsutsumi, H. Nakamori, and K. Ichikawa, Phys. Rev. B **13**, 929 (1976).
[51] M. Deutsch, G. Hölzer, J. Härtwig, J. Wolf, M. Fritsch, and E. Förster, Phys. Rev. A **51**, 283 (1995).
[52] Y.-F. Song, S.-B. Lee, and C.-N. Chang, Chin. J. Phys. **33**, 671 (1995).
[53] H. Enkisch, C. Sternemann, M. Paulus, M. Volmer, and W. Schülke, Phys. Rev. A **70**, 022508 (2004).
[54] M. Deutsch, E. Förster, G. Hölzer, J. Härtwig, K. Hämäläinen, C.-C. Kao, S. Huotari, and R. Diamant, J. Res. Natl. Inst. Stand. Technol. **109**, 75 (2004).
[55] B. G. Gokhale, S. Rai, and S. D. Rai, J. Phys. F **7**, 299 (1977).
[56] I. Török, T. Papp, J. Pálinkás, M. Budnar, A. Mühleisen, J. Kawai, and J. L. Campbell, Nucl. Instrum. Methods B **114**, 9 (1996).
[57] R. Bonetto, G. Castellano, and J. Trincavelli, X-Ray Spectrom. **30**, 313 (2001).
[58] S. Limandri, R. Bonetto, H. Di Rocco, and J. Trincavelli, Spectrochim. Acta B **63**, 962 (2008).
[59] J. Trincavelli and G. Castellano, Spectrochim. Acta B **63**, 1 (2008).
[60] J. Trincavelli, S. Limandri, A. Carreras, and R. Bonetto, Microsc. Microanal. **14**, 306 (2008).
[61] S. P. Limandri, J. C. Trincavelli, R. D. Bonetto, and A. C. Carreras, Phys. Rev. A **78**, 022518 (2008).
[62] J. A. Bearden, Rev. Mod. Phys. **39**, 78 (1967).
[63] J. A. Bearden and A. F. Burr, Rev. Mod. Phys. **39**, 125 (1967).
[64] S. T. Perkins, D. E. Cullen, M. H. Chen, J. H. Hubbell, J. Rathkopf, and J. Scofield, Lawrence Livermore National Laboratory Report No. UCRL-50400, 1991, Vol. 30.
[65] E. Margeter, W. Wegscheider, and K. Müller, X-Ray Spectrom. **13**, 78 (1984).
[66] O. Ford, Phys. Rev. **41**, 577 (1932).
[67] A. Servomaa and O. Keski-Rahkonen, J. Phys. C **8**, 4124 (1975).
[68] O. Keski-Rahkonen and J. Ahopelto, J. Phys. C **13**, 471 (1980).
[69] S. A. E. Johansson, J. L. Campbell, and K. G. Malmqvist, *Particle Induced X-ray Emission Spectrometry PIXE* (Wiley, New York, 1995), p. 34.
[70] M. Bé, M. Lépy, J. Plagnard, and B. Duchemin, Appl. Radiat. Isot. **49**, 1367 (1998).
[71] E. Mikkola, O. Keski-Rahkonen, J. Lahtinen, and K. Reinikainen, Phys. Scr. **28**, 188 (1983).
[72] F. M. F. de Groot, A. Fontaine, C. C. Kao, and M. Krisch, J. Phys.: Condens. Matter **6**, 6875 (1994).
[73] G. Peng, F. M. F. de Groot, K. Hämäläinen, J. A. Moore, X. Wang, M. M. Grush, J. B. Hastings, D. P. Siddons, W. H. Armstrong, O. C. Mullins, and S. P. Cramer, J. Am. Chem. Soc. **116**, 2914 (1994).
[74] R. E. LaVilla, Phys. Rev. A **19**, 717 (1979).
[75] E. Asada, T. Takiguchi, and Y. Suzuki, X-Ray Spectrom. **4**, 186 (1975).

[76] M. A. Blokhin and I. G. Svejcer, *Rentgenospektralny Spravochnik* (Nauka, Moscow, 1982), Table 12.1, p. 70.
[77] H.-T. Meyer, Wiss. Veröff. Siemens-Konzern **7**, 108 (1929).
[78] R. D. Deslattes *et al.*, X-ray Transition Energies (Version 1.2), National Institute of Standards and Technology, Gaithersburg, MD, 2005. Originally published as: R. D. Deslattes, E. G. Kessler, Jr., P. Indelicato, L. de Billy, E. Lindroth, and J. Anton, Rev. Mod. Phys. **75**, 35 (2003). [Online at http://www.physics.nist.gov/XrayTrans (October, 2009)].
[79] California Institute of Technology (CALTECH), Division of Physics, Mathematics & Astronomy. [Online at http://www.pma.caltech.edu/∼dons/ph3–7/xray. dat (September, 1997)].